EUROPEAN ORGANIZATION FOR NUCLEAR RESEARCH

L3 Note 2555
June 28, 2000

QCD Results at $\sqrt{s} \geq 192$ GeV

The L3 Collaboration

Abstract

We present preliminary results obtained from a study of the structure of hadronic events recorded by the L3 detector at centre-of-mass energies $\sqrt{s} \geq 192$ GeV. The jet rates at these energies at different jet resolution parameters have been compared with predictions of various QCD models. The distributions of event shape variables and the energy dependence of their mean values are compared with the QCD models. The energy dependence of the moments of event shape variables is used to test a power law ansatz for the non-perturbative component. We obtain a universal value of the non-perturbative parameter $\alpha_0 = 0.482 \pm 0.065$. From a comparison with resummed $\mathcal{O}(\alpha_s^2)$ QCD calculations, we determine the strong coupling constant at these energies. The measurements demonstrate the running of α_s as expected in QCD with a value of $\alpha_s(m_Z) = 0.1218 \pm 0.0012$ (exp) $\pm\ 0.0061$ (th). The charged particle multiplicity distributions and inclusive momentum spectra are studied and the energy dependence of the peak position of the ξ $(= -\ln x)$ distribution is compared with lower energy measurements and QCD expectations.

Submitted to the *XXXth International Conference on High Energy Physics*
July 27 - August 2, 2000, Osaka, Japan

1 Introduction

Hadronic events produced in e^+e^- annihilation offer a good environment to test the predictions of the theory of the strong interaction (QCD). It is also worthwhile to check the validity of the QCD models very often used in particle searches and other studies. LEP operated at four different centre-of-mass energies in 1999: 192, 196, 200 and 202 GeV and in a range of centre-of-mass energies between 202 and 208 GeV in the year 2000.

We report here measurements of event shape distributions and their moments using the data collected with the L3 detector [1]. To allow a direct comparison with our earlier QCD tests done at lower energies [2–5], we follow an identical analysis procedure. For the ease of comparison we have combined measurements at neighbouring centre-of-mass energies. This leaves us with 3 samples with mean energies of 195.0 GeV (192 + 196 GeV) and 200.6 GeV (200 + 202 GeV) from the 1999 data and 205.3 GeV from the 2000 data.

The measured distributions are compared with predictions from event generators based on an improved leading log approximation (Parton Shower models including QCD coherence effects). Three such Monte Carlo programs (Ariadne [6], Herwig [7] and Jetset PS [8]) have been used for these comparisons. We also compare our measurements with prediction from QCD models with no coherence effects (Cojets [9]). These Monte Carlo programs use different approaches to describe both the perturbative parton shower evolution and non-perturbative hadronisation processes. They have been tuned [10] to reproduce the global event shape distributions and the charged particle multiplicity distribution measured at 91.2 GeV [2].

The moments of event shape variables are measured at the three mean energy points. The perturbative and non-perturbative QCD contributions are obtained from a fit using the power correction formula [11] to all our measurements.

The strong coupling constant α_s is extracted at each of these centre-of-mass energies by comparing the measured event shape distributions with predictions of second order QCD calculations [12] with resummed leading and next-to-leading order terms [13].

We include the measurement of the charged particle multiplicity distributions and the peak positions, $\xi^\star$, of the charged particle ξ $(= -\ln x)$ spectra at the three mean centre-of-mass energies together with similar measurements at lower energies.

Section 2 describes the selection of hadronic events. The measurement of jet rates in hadronic events are summarised in section 3. Measurements of event shape variables and estimation of systematic errors are described in section 4. Section 5 presents a comparison of the event shape measurements with predictions from various QCD models, a study of the power correction ansatz and a determination of α_s from event shape distributions. Results on charged particle multiplicities and inclusive spectra are discussed in sections 6 and 7. The results are summarised in section 8.

2 Event Selection

The selection of $e^+e^- \rightarrow$ hadrons events is based on the energy measured in the electromagnetic and hadron calorimeters. We use energy clusters in the calorimeters with a minimum energy of 100 MeV. We measure the total visible energy (E_{vis}) and the energy imbalances parallel ($E_{\parallel}$) and perpendicular ($E_{\perp}$) to the beam direction.

We use Monte Carlo events to estimate the efficiency of the selection criteria and purity of the data sample. Monte Carlo events for the process $e^+e^- \rightarrow q\bar{q}(\gamma)$ have been generated by the parton shower program Kk2f [14] and passed through the L3 detector simulation [15].

The background events are simulated with appropriate event generators: PYTHIA [16] and PHOJET [17] for two-photon events, KORALZ [18] for the $\tau^+\tau^-(\gamma)$ final state, BHAGENE [19] and BHWIDE [20] for Bhabha events, KORALW [21] for W-pair production and PYTHIA for Z-pair production.

The multi-hadronic final states are selected with simple cuts on the visible energy, energy imbalances and cluster multiplicity (N_{cl}) as described in [2,4,5]. At high energies, the dominant background comes from ISR where the mass of the resulting hadronic system is close to m_{Z}. This background is reduced by applying a cut in the two dimensional plane of $\mid E_{\parallel} \mid / E_{\mathrm{vis}}$ and $E_{\mathrm{vis}}/\sqrt{s}$. There are additional backgrounds arising from W-pair and Z-pair production. Substantial fraction of these events can be removed by a specific selection as described in [5]. The selection is based on:

- forcing the event to a 4-jet topology using the Durham algorithm [22],
- performing a kinematic fit imposing the constraints of energy-momentum conservation,
- making cuts on energies of the most and the least energetic jets and on y_{34}^{D}, where y_{34}^{D} is the jet resolution parameter for which the event is classified as a three-jet rather than a four-jet event.

These cuts have also been optimised at each energy point. Hadronic events with ISR photon energy larger than $0.18\sqrt{s}$ are considered as background.

The integrated luminosity, selection efficiency, purity and number of selected events for each of the energy points are summarised in Table 1.

$<\sqrt{s}>$ (GeV)	195.0	200.6	205.3
Integrated Luminosity (pb^{-1})	112.2	117.0	56.7
Selection Efficiency (%)	82.7	82.6	83.3
Sample Purity (%)	83.3	81.8	80.6
Selected Events	2403	2373	1167
Expected Events	2415	2370	1085

Table 1: Summary of integrated luminosity, selection efficiency, sample purity and number of selected and expected hadronic events at the different energies used in this analysis.

3 Jet Rates

Jets are reconstructed using the JADE algorithm [23]. For each pair of particles i and j the expression:

$$y_{ij} = \frac{2E_iE_j}{s}(1-\cos\theta_{ij})$$

is evaluated. E_i and E_j are their energies and θ_{ij} is the angle between them. The pair for which y_{ij} is the smallest is replaced by a pseudo-particle l with four momentum

$$p_l = p_i + p_j \,.$$

This procedure is repeated until all y_{ij} exceed the jet resolution parameter y_{cut}. The remaining pseudo-particles are called jets. The jet fraction f_i is the fraction of all hadronic events containing i-jets

$$f_i = \frac{\sigma_{i-jets}}{\sigma_{tot}}$$

Figure 1 shows the distribution of f_i at detector level as a function of jet-multiplicity i at $\sqrt{s}$ = 195.0 GeV for $y_{cut} = 0.08$. As can be seen the data are in good agreement with predictions from parton shower Monte Carlo program JETSET.

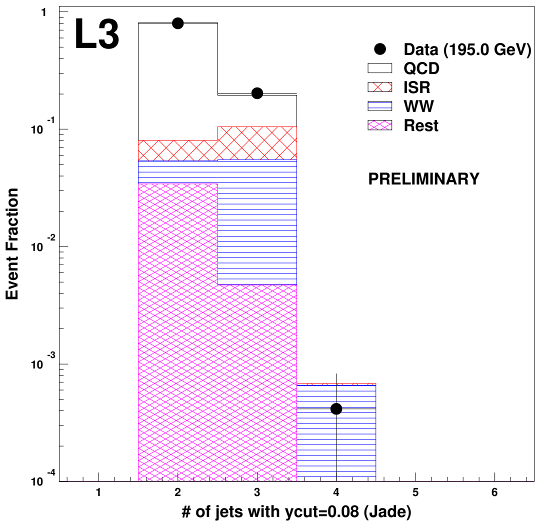

Figure 1: Jet rate at detector level at mean centre-of-mass energy of 195.0 GeV for $y_{cut} = 0.08$ using the JADE algorithm compared with predictions of QCD model.

Figure 2 shows the corrected jet rates as a function of the jet resolution parameter y_{cut} for 2-, 3-, 4- and 5-jets at $< \sqrt{s} >$ = 200.6 GeV where the jets are reconstructed using the Durham algorithm [22]. This algorithm closely follows the JADE algorithm with the difference that the closeness variable y_{ij} between two particles is defined somewhat differently to take care of summing up soft gluon emission:

$$y_{ij} = \frac{2\min(E_i^2, E_j^2)}{s}(1 - \cos\theta_{ij})$$

Again the data are well described by the different parton shower models.

In the Cambridge algorithm [24] one has isolated the ordering parameter for combining particles into pseudo-particles from the jet resolution parameter. In this algorithm, the ordering parameter v_{ij} is chosen to be

$$v_{ij} = (1 - \cos\theta_{ij}) \ .$$

The pair for which v_{ij} is the smallest is examined first. The concept of soft freezing is introduced which states that if y_{ij} is smaller than y_{cut}, the particles i and j are combined to form a pseudo-particle l as in the previous two algorithms, but if y_{ij} is larger than y_{cut}, the smaller energy object (between i and j) is frozen as a jet. Figure 3 shows the corrected jet rates for Cambridge algorithm as a function of the jet resolution parameter y_{cut} for 2-, 3-, 4- and 5-jets at $< \sqrt{s} >$ = 205.3 GeV. The different QCD models give a satisfactory description of the measured rates within their uncertainties.

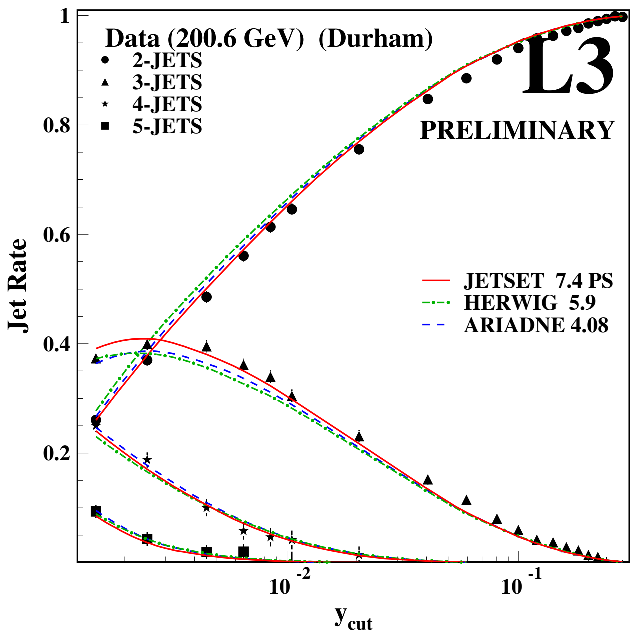

Figure 2: Corrected jet rate at $<\sqrt{s}> = 200.6$ GeV for 2-, 3-, 4- and 5-jet events using the Durham algorithm compared with predictions of various QCD models.

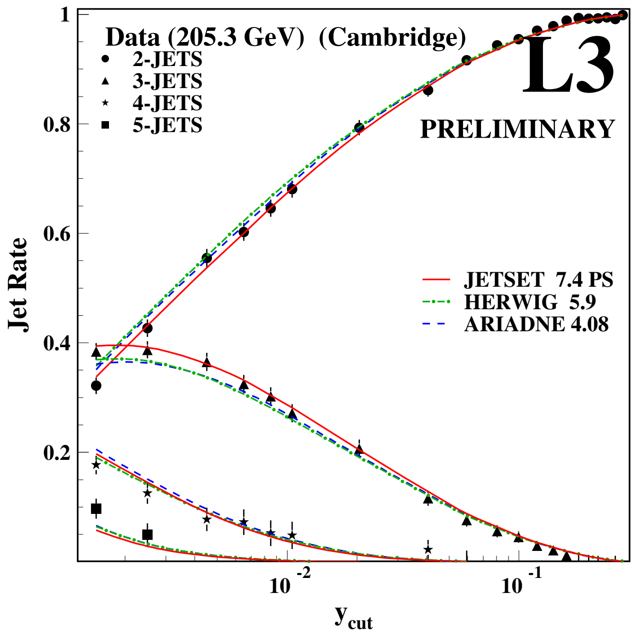

Figure 3: Corrected jet rate at $<\sqrt{s}> = 205.3$ GeV for 2-, 3-, 4- and 5-jet events using the Cambridge algorithm compared with predictions of various QCD models.

4 Measurement of Event Shape Variables

We measure five global event shape variables for which improved analytical QCD calculations [13] are available. These are thrust (T), scaled heavy jet mass (ρ), total (B_T) and wide (B_W) jet broadening variables and the C-parameter.

For Monte Carlo events, the global event shape variables are calculated before (particle level) and after (detector level) detector simulation. The calculation before detector simulation takes into account all stable charged and neutral particles. The measured distributions at detector level differ from the ones at particle level because of detector effects, limited acceptance and resolution. After subtracting the background obtained from simulations, the measured distributions are corrected for detector effects, acceptance and resolution on a bin-by-bin basis by comparing the detector level results with the particle level results. The level of migration is kept at a negligible level with a bin size larger than the experimental resolution. We also correct the data for initial and final state photon radiation bin-by-bin using Monte Carlo distributions at particle level with and without radiation.

The systematic uncertainties in the distributions of event shape variables arise mainly due to uncertainties in the estimation of detector correction and background estimation. The uncertainty in the detector correction has been estimated by several independent checks:

- The definition of reconstructed objects used to calculate the observables has been changed. Instead of using only calorimetric clusters, the analysis has been repeated with objects obtained from a non-linear combination of energies of charged tracks and calorimetric clusters.

- The effect of different particle densities in correcting the measured distribution has been estimated by changing the signal Monte Carlo program (HERWIG instead of JETSET).

- The acceptance has been reduced by restricting the events to the central part of the detector ($|\cos(\theta_{\mathrm{T}})| < 0.7$, where θ_{T} is the polar angle of the thrust axis relative to the beam direction) where the energy resolution is better.

The uncertainty on the background composition of the selected event sample has been estimated by repeating the analysis with:

- an alternative criterion to reject the hard initial state photon events based on a cut on the kinematically reconstructed effective centre-of-mass energy,

- a variation of the estimated two-photon interaction background by $\pm$ 30% and by changing the background Monte Carlo program (PHOJET instead of PYTHIA), and

- a variation of the $\mathrm{W^+W^-}$ background estimate by changing the W-pair rejection criteria.

The systematic uncertainties obtained from different sources are combined in quadrature. Uncertainties due to ISR and $\mathrm{W^+W^-}$ backgrounds are the most important ones. They are roughly equal and are 2-3 times larger than the uncertainties due to the detector correction. Statistical fluctuations are not negligible in the estimation of systematic effects. The statistical component of the systematic uncertainty is determined by splitting the overall Monte Carlo sample into luminosity weighted sub-samples and treating each of these sub-samples as data. The spread in the mean position gives an estimate of the statistical component and is taken out from the original estimate in quadrature.

5 Results on Event Shape Measurements

5.1 Comparison with QCD models

Figures 4 and 5 show the corrected thrust and wide jet broadening distributions obtained at mean centre-of-mass energies of 195.0, 200.6 and 205.3 GeV. The data are compared with Jetset, Herwig and Ariadne QCD models at particle level. The agreement is satisfactory.

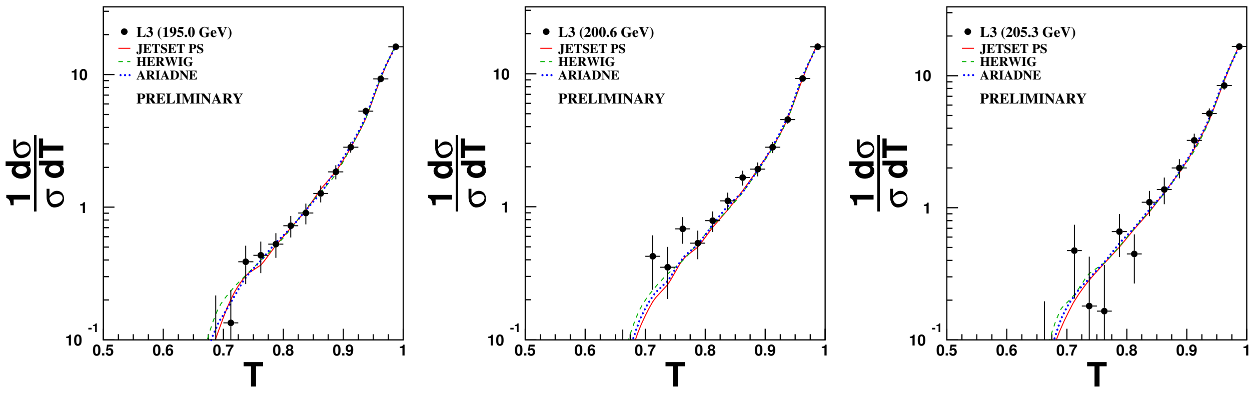

Figure 4: Corrected distributions for thrust, T, at 195.0, 200.6 and 205.3 GeV in comparison with QCD model predictions. The errors shown are statistical only.

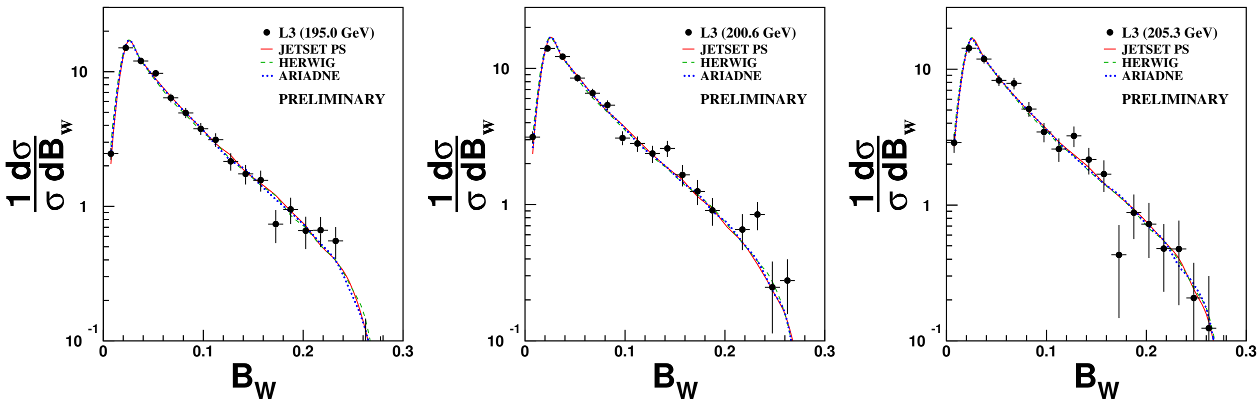

Figure 5: Corrected distributions for wide jet broadening, B_W, at 195.0, 200.6 and 205.3 GeV in comparison with QCD model predictions. The errors shown are statistical only.

An important test of QCD models is a comparison of the energy evolution of the event shape variables. The energy dependence of the mean event shape variables arises mainly from two sources: the logarithmic energy scale dependence of α_s and the power law behaviour of non-perturbative effects. The first moments of the five event shape variables are shown in Figure 6 including our previous measurements and in Table 2. Also shown are the energy dependences of these quantities as predicted by Jetset PS, Herwig, Ariadne, Cojets and Jetset ME ($\mathcal{O}(\alpha_s^2)$ matrix element implementation). All the models with the possible exception of Jetset ME give a good description of the data.

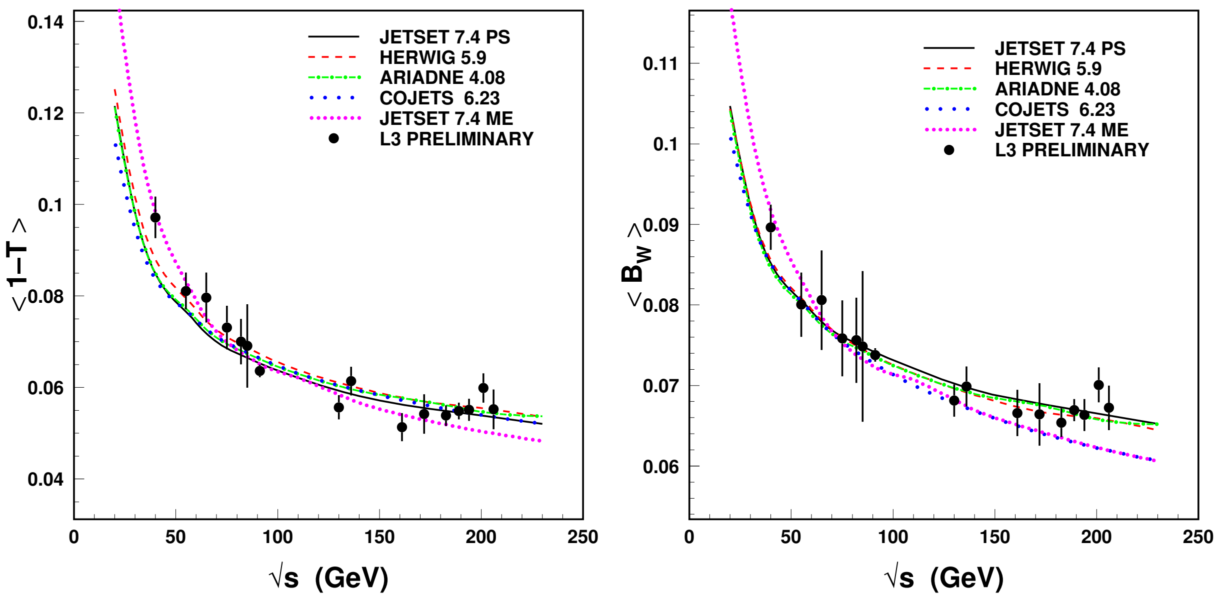

Figure 6: Distribution of mean 1−thrust, $< 1 - T >$ and wide jet broadening, $< B_W >$ as a function of the centre-of-mass energy, compared to several QCD models.

$< \sqrt{s} >$	195.0 GeV	200.6 GeV	205.3 GeV
$< (1-T) >$	$.0551 \pm .0018 \pm .0016$	$.0599 \pm .0021 \pm .0024$	$.0552 \pm .0030 \pm .0032$
$< \rho >$	$.0439 \pm .0013 \pm .0013$	$.0480 \pm .0015 \pm .0013$	$.0449 \pm .0021 \pm .0020$
$< B_T >$	$.0920 \pm .0019 \pm .0029$	$.0964 \pm .0021 \pm .0026$	$.0927 \pm .0032 \pm .0030$
$< B_W >$	$.0663 \pm .0013 \pm .0015$	$.0701 \pm .0014 \pm .0016$	$.0672 \pm .0021 \pm .0018$
$< C >$	$.2158 \pm .0052 \pm .0046$	$.2281 \pm .0059 \pm .0071$	$.2161 \pm .0089 \pm .0092$

Table 2: First moments of the five event shape variables at different energy points. The two errors are respectively statistical and systematic.

5.2 Power Law Correction Analysis

The energy dependence of moments of the event shape variables has been described [11] as a sum of the perturbative contributions and a power law dependence due to non-perturbative contributions. The first moment of an event shape variable f is written as

$$\langle f \rangle \;=\; \langle f_{\mathrm{pert}} \rangle + \langle f_{\mathrm{pow}} \rangle \,, \tag{1}$$

where the perturbative contribution $\langle f_{\mathrm{pert}} \rangle$ has been determined to $\mathcal{O}(\alpha_{\mathrm{s}}^2)$ [25]. The power correction term [11], for $1-T$, ρ, and C, is given by

$$\langle f_{\mathrm{pow}} \rangle \;=\; c_f \mathcal{P} \,, \tag{2}$$

where the factor c_f depends on the shape variable f and $\mathcal{P}$ is supposed to have a universal form:

$$\mathcal{P} \;=\; \frac{4C_F}{\pi^2}\mathcal{M}\frac{\mu_I}{\sqrt{s}}\left[\alpha_0(\mu_I) - \alpha_{\mathrm{s}}(\sqrt{s}) - \beta_0\frac{\alpha_{\mathrm{s}}^2(\sqrt{s})}{2\pi}\left(\ln\frac{\sqrt{s}}{\mu_I} + \frac{K}{\beta_0} + 1\right)\right] \tag{3}$$

for a renormalisation scale fixed at $\sqrt{s}$. The parameter α_0 is related to the value of α_{s} in the non-perturbative region below an infrared matching scale μ_I (= 2 GeV); β_0 is $(11N_c - 2N_f)/3$, where N_c is the number of colours and N_f is the number of active flavours. $K = (67/18 - \pi^2/6)C_A - 5N_f/9$ and C_F, C_A are the usual colour factors. The Milan factor $\mathcal{M}$ is 1.49 for N_f = 3. For the jet broadening variables, the power correction term takes the form

$$\langle f_{\mathrm{pow}} \rangle \;=\; c_f F \mathcal{P} \,, \tag{4}$$

where

$$F \;=\; \left(\frac{\pi}{2\sqrt{aC_F\alpha_{\mathrm{CMW}}}} + \frac{3}{4} - \frac{\beta_0}{6a\ C_F} - 0.6137 + \mathcal{O}(\sqrt{\alpha_{\mathrm{s}}})\right) \tag{5}$$

and a takes a value 1 for B_T and 2 for B_W and α_{CMW} is related to α_{s} [11].

We have carried out fits to the first moments of the five event shape variables, together with our earlier measurements [5], separately with $\alpha_{\mathrm{s}}(m_{\mathrm{Z}})$ and α_0 as free parameters. The diagonal terms of the covariance matrix between the different energy points are constructed by summing in quadrature the systematic uncertainty and the statistical error. The off-diagonal terms are obtained from the common systematic errors. The results of the fits are summarised in Table 3 and shown in Figure 7.

The five values of α_0 obtained from the event shape variables agree within errors, supporting the predicted universality of the power law behaviour. The five estimates of α_0 and α_{s} are combined by taking an unweighted average to obtain the overall fitted values:

$$\alpha_0 \;=\; 0.482 \;\pm\; 0.062 \;\pm\; 0.021 \,, \tag{6}$$

$$\alpha_{\mathrm{s}}(m_{\mathrm{Z}}) \;=\; 0.1139 \;\pm\; 0.0043 \;\pm\; 0.0034 \,. \tag{7}$$

The first error on each measurement is experimental and is obtained from the average of the five errors on α_0 and α_{s}. To estimate theoretical uncertainties we vary the renormalisation scale between $0.5\sqrt{s}$ and $2.0\sqrt{s}$ and α_0 and $\alpha_{\mathrm{s}}(m_{\mathrm{Z}})$ vary on average by ±0.021 and ±0.0033 respectively. A variation of μ_I in the range from 1 to 3 GeV gives an additional uncertainty

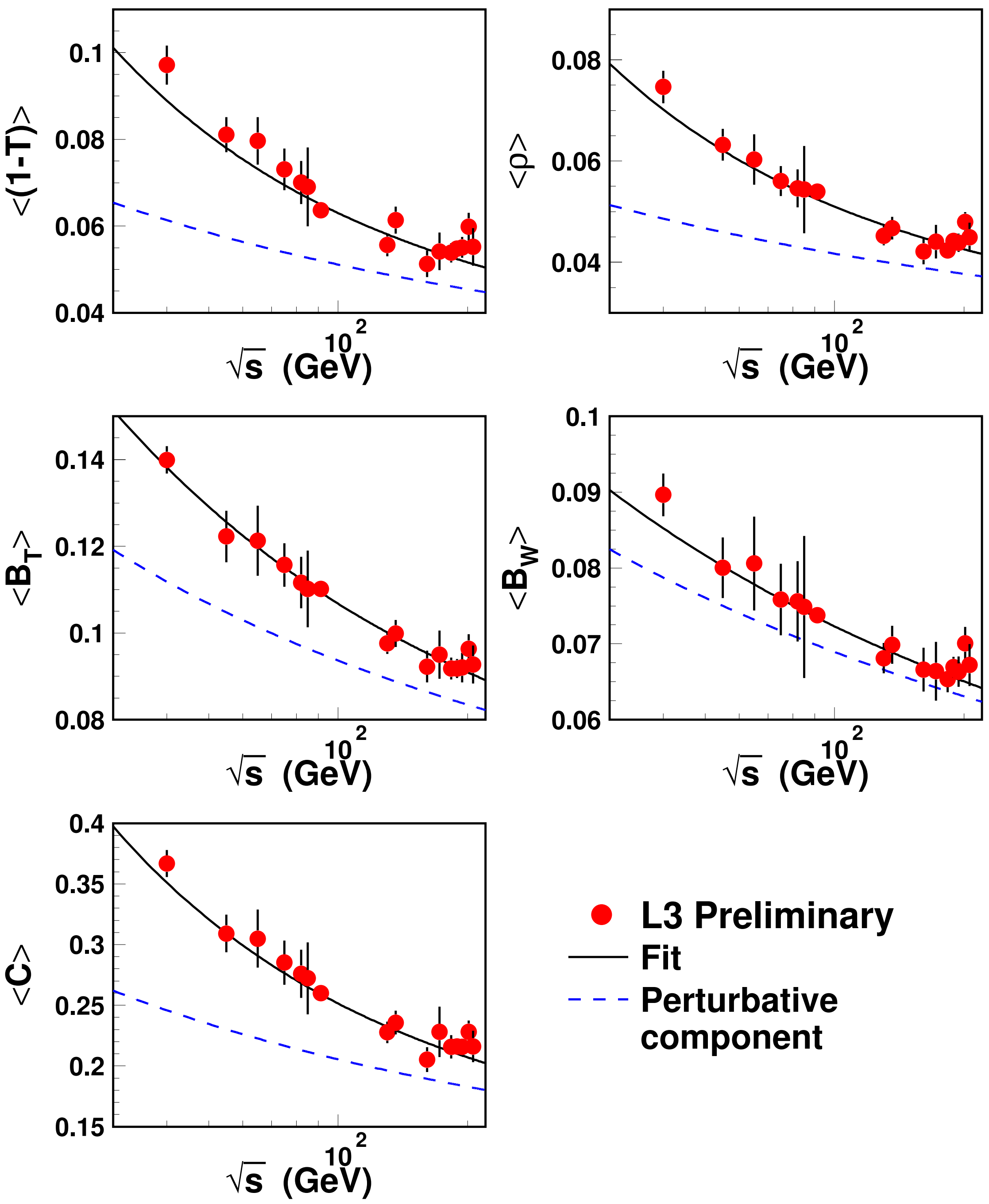

Figure 7: The first moments of the five event shape variables, $1-T$, ρ, B_T, B_W and C compared to the results of a fit including perturbative and power law contributions.

Observable	α_0	$\alpha_s(m_Z)$	χ^2/d.o.f.	A_2 (GeV^2)
$1-T$	0.566 ± 0.063	0.1147 ± 0.0063	24.8/14	4.58 ± 0.55
ρ	0.467 ± 0.055	0.1067 ± 0.0045	14.0/14	$0.00\ ^{+0.01}_{-0.00}$
B_T	0.491 ± 0.044	0.1173 ± 0.0029	7.6/14	13.73 ± 0.87
B_W	0.387 ± 0.105	0.1164 ± 0.0043	9.8/14	$0.00\ ^{+0.01}_{-0.00}$
C	0.499 ± 0.042	0.1144 ± 0.0036	15.2/14	11.04 ± 0.80

Table 3: Determination of α_0 and $\alpha_s(m_Z)$ from fits to the first moments of the event shape distributions together with χ^2/d.o.f. from those fits. Also shown is the A_2 parameter from fits to the second moments.

on $\alpha_s(m_Z)$ of $\pm$ 0.0010. These two estimates of theoretical uncertainties are combined in quadrature and quoted as the second error.

We have also measured the second moments of these shape variables which are summarised in Table 4. The energy dependence of these moments has been analysed in terms of power law corrections. For variables $1-T$, ρ and C, the following result is expected to hold [26]:

$$\langle f^2 \rangle \;=\; \langle f^2_{\mathrm{pert}} \rangle \;+\; 2\langle f_{\mathrm{pert}} \rangle c_f \mathcal{P} \;+\; \mathcal{O}\left(\frac{1}{s}\right) \,. \tag{8}$$

This assumes that the non-perturbative correction to the distributions causes only a shift. For jet broadenings the power corrections are more complicated. The $\mathcal{O}(\frac{1}{s})$ term has been parametrised as A_2/s and is expected to be small for $1-T$, ρ and C. Fits have been performed to the second moments including our previous measurements [5]. Here α_0 and α_s have been fixed to the values obtained from the corresponding fits to the first moments. Figure 8 shows the second moments compared to these fits. The contributions of the $\mathcal{O}(\frac{1}{s})$ term are non-negligible for $1-T$ and C, in contradiction with the expectation. The five values of A_2, as obtained from the fits, are summarised in Table 3.

$< \sqrt{s} >$	195.0 GeV	200.6 GeV	205.3 GeV
$< (1-T)^2 >$	$.0063 \pm .0005 \pm .0004$	$.0078 \pm .0006 \pm .0005$	$.0065 \pm .0008 \pm .0011$
$< \rho^2 >$	$.0042 \pm .0003 \pm .0002$	$.0052 \pm .0003 \pm .0003$	$.0044 \pm .0005 \pm .0004$
$< B_T^2 >$	$.0122 \pm .0006 \pm .0010$	$.0136 \pm .0007 \pm .0007$	$.0124 \pm .0010 \pm .0010$
$< B_W^2 >$	$.0069 \pm .0003 \pm .0003$	$.0079 \pm .0003 \pm .0003$	$.0070 \pm .0005 \pm .0004$
$< C^2 >$	$.0778 \pm .0040 \pm .0032$	$.0896 \pm .0047 \pm .0054$	$.0787 \pm .0072 \pm .0091$

Table 4: Second moments of the five event shape variables at different energy points. The two errors are respectively statistical and systematic.

5.3 α_s from Event Shape Distributions

In order to derive α_s from event shape variables at each energy point we fit the measured distributions to theoretical calculations based on $\mathcal{O}(\alpha_s^2)$ perturbative QCD with resummed leading and next-to-leading order terms. These calculations are performed at parton level and do not include heavy quark mass effects. To compare the analytical calculations with the experimental distributions, the effects of hadronisation and decays have been corrected for using Monte Carlo programs.

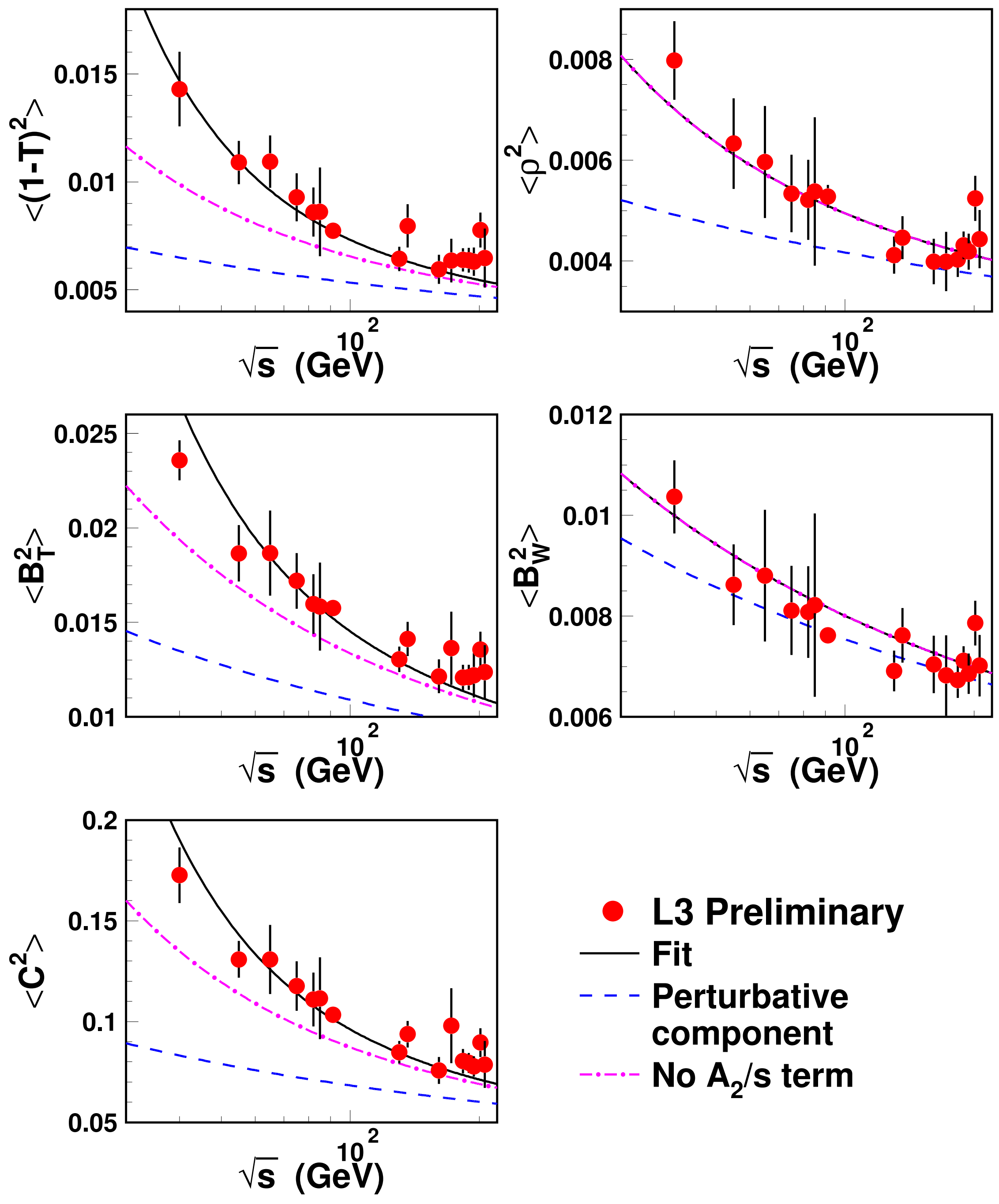

Figure 8: The second moments of the five event shape variables, $1-T$, ρ, B_T, B_W and C compared to the results of a fit including perturbative and power law contributions. The parameters α_0 and α_s are fixed to the values obtained by the fits to the first moments. The A_2/s term is negligible for ρ and B_W but is necessary to reproduce the behaviour of $1-T$, B_T and C.

The fit ranges used take into account the limited statistics at high energy as well as the reliability of the resummation calculation and are given in Table 5. In this analysis, we determine α_s at $<\sqrt{s}>$ = 195.0, 200.6 and 205.3 GeV. All the measurements are summarised in Table 5.

	$(1-T)$	ρ	B_T	B_W	C
Fit Range	0.00−0.30	0.00−0.20	0.00−0.25	0.00−0.20	0.05−0.50
α_s(195.0 GeV)	0.1168	0.1096	0.1116	0.1032	0.1130
Statistical error	±0.0019	±0.0017	±0.0014	±0.0013	±0.0023
Systematic error	±0.0015	±0.0014	±0.0011	±0.0013	±0.0024
Overall experimental error	±0.0024	±0.0022	±0.0018	±0.0018	±0.0033
Overall theoretical error	±0.0056	±0.0039	±0.0065	±0.0062	±0.0056
χ^2/d.o.f.	2.4 / 10	7.2 / 9	26.7 / 11	8.8 / 12	3.8 / 8
α_s(200.6 GeV)	0.1182	0.1111	0.1127	0.1033	0.1146
Statistical error	±0.0021	±0.0017	±0.0014	±0.0014	±0.0024
Systematic error	±0.0031	±0.0030	±0.0023	±0.0018	±0.0027
Overall experimental error	±0.0038	±0.0034	±0.0027	±0.0023	±0.0036
Overall theoretical error	±0.0059	±0.0034	±0.0065	±0.0062	±0.0057
χ^2/d.o.f.	7.9 / 9	9.7 / 13	19.2 / 11	15.5 / 12	3.4 / 8
α_s(205.3 GeV)	0.1160	0.1108	0.1127	0.1043	0.1121
Statistical error	±0.0029	±0.0026	±0.0022	±0.0020	±0.0039
Systematic error	±0.0021	±0.0024	±0.0019	±0.0017	±0.0029
Overall experimental error	±0.0036	±0.0035	±0.0029	±0.0026	±0.0049
Overall theoretical error	±0.0056	±0.0034	±0.0065	±0.0068	±0.0053
χ^2/d.o.f.	7.0 / 9	17.5 / 13	11.2 / 11	13.5 / 12	9.0 / 8

Table 5: α_s measured at $<\sqrt{s}>$ = 195.0, 200.6 and 205.3 GeV from fits of the event shape variables to theoretical predictions with combined fixed order and resummed calculations. The fit ranges, the estimated experimental and theoretical errors and the fit quality are also given.

The experimental errors include the statistical errors and the experimental systematic uncertainties. The theoretical error is obtained from estimates [5] of the hadronisation uncertainty and of the errors coming from the uncalculated higher orders in the QCD predictions. The estimate of the theoretical error does not always reflect the true size of uncalculated higher order terms. An independent estimate is obtained from a comparison of α_s measurements from many event shape variables which are affected differently by higher order corrections and hadronisation effects. To obtain a combined value for the strong coupling constant we take the unweighted average of the five α_s values. We estimate the overall theoretical error from the simple average of the five theoretical errors or from half of the maximum spread in the five α_s values. Both estimates yield similar results. The combined results are summarised in Table 6. The earlier measurements at $\sqrt{s} = m_Z$ and at reduced centre-of-mass energies determined α_s from four event shape variables only: T, ρ, B_T and B_W. For comparison we also provide in Table 6 the mean from these four measurements.

We compare the energy dependence of the measured α_s values, together with our previous measurements, with the prediction from QCD in Figure 9. The theoretical errors are strongly correlated between these measurements. The error appropriate to a measurement of the energy dependence of α_s can then be considered to be experimental. The experimental systematic errors on α_s are dominated by the background uncertainties. These are similar for all the individual low energy or high energy data points but differ between the low energy, Z peak and

$<\sqrt{s}>$ (GeV)	α_s (from T, ρ, B_T, B_W)	α_s (from T, ρ, B_T, B_W, C)
195.0	$0.1103 \pm 0.0021 \pm 0.0056$	$0.1108 \pm 0.0023 \pm 0.0056$
200.6	$0.1113 \pm 0.0031 \pm 0.0055$	$0.1120 \pm 0.0032 \pm 0.0056$
205.3	$0.1110 \pm 0.0031 \pm 0.0056$	$0.1112 \pm 0.0035 \pm 0.0055$

Table 6: Summary of α_s values as determined from event shape variables at different centre-of-mass energies.

high energy data sets. The experimental systematic errors are then different and uncorrelated between the three data sets, but are taken as fully correlated between individual low energy or high energy measurements. The sixteen measurements in Figure 9 are shown with experimental errors only, together with a fit to the QCD evolution equation [27] with $\alpha_s(m_Z)$ as a free parameter. The fit gives a χ^2 of 17.3 for 15 degrees of freedom corresponding to a confidence level of 0.30 with a fitted value of α_s:

$$\alpha_s(m_Z) = 0.1218 \pm 0.0012 \pm 0.0061 . \tag{9}$$

The first error is experimental and the second error is theoretical. On the other hand, a fit with constant α_s gives a χ^2 of 66.2 for 15 degrees of freedom. The value of $\alpha_s(m_Z)$ thus obtained is in agreement with the value obtained in the power law ansatz analysis considering the experimental and the theoretical uncertainties. These measurements support the energy evolution of the strong coupling constant predicted by QCD.

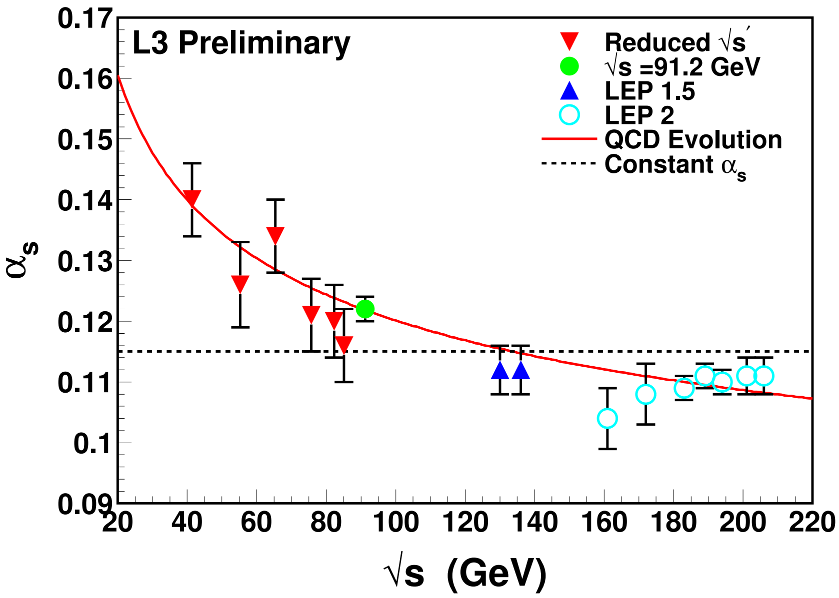

Figure 9: α_s measurements from event shape distributions as a function of the centre-of-mass energy. The errors shown are experimental only. The solid and dashed lines are fits with the energy dependence of α_s as expected from QCD and with constant α_s, respectively.

The slope in the energy evolution of α_s depends on the number of active flavours. We have performed a fit with N_f as a free parameter along with α_s and obtain the number of active flavours:

$$N_f \;=\; 5.1 \;\pm\; 1.3 \;\pm\; 1.9\;, \tag{10}$$

where the first error is experimental and the second is due to theoretical uncertainties. The errors have been estimated by using the covariance matrix determined from experimental and overall errors on α_{s} in the fit. This result agrees with the expectation $N_f = 5$.

6 Charged Particle Multiplicity

The dynamics of hadron production can be probed using the charged particle multiplicity distribution which has been found to be very sensitive to the parameters of the QCD models.

The measured distributions are corrected for the remaining estimated background using Monte Carlo on a bin-by-bin basis. The distributions are then corrected for resolution and acceptance, using a matrix unfolding method. In this correction procedure, we assume all weakly decaying light particles with mean lifetime larger than 3.3×10^{-10} s to be stable.

The systematic errors have been determined in the same manner as for the global event shape variables with one additional contribution corresponding to a variation of the quality criteria for track selection.

The mean charged particle multiplicities, $\langle \mathrm{n_{ch}} \rangle$, at $\sqrt{s} \geq 189$ GeV are summarised in Table 7. The first error refers to the statistical uncertainty and the second error refers to the systematic uncertainty. We also include the measurement done at $\sqrt{s} = 189$ GeV from the data collected by L3 during 1998.

$<\sqrt{s}>$ (GeV)	$\langle \mathrm{n_{ch}} \rangle$
189.0	$26.84 \pm 0.20 \pm 0.25$
195.0	$27.10 \pm 0.25 \pm 0.32$
200.6	$27.45 \pm 0.23 \pm 0.35$
205.3	$28.37 \pm 0.48 \pm 0.93$

Table 7: Mean charged particle multiplicity measured at different centre-of-mass energies

Figure 10 shows the evolution of mean charged particle multiplicity with centre-of-mass energy compared to several QCD models. We also include measurements done by $\mathrm{e^+e^-}$ experiments at similar [2, 4, 5, 28, 29] and lower [30] centre-of-mass energies. The parameters of these models are the same at all energies. We find that the energy dependence of the multiplicity distribution is in agreement with the predictions of parton shower models like Jetset, Herwig, Ariadne which include QCD coherence effects. However, parton shower models with no QCD coherence effects like Cojets or matrix element models as implemented in Jetset cannot explain the energy dependence. Cojets predicts a faster energy evolution, while the matrix element model, which has low parton multiplicity before fragmentation due to $\mathcal{O}(\alpha_{\mathrm{s}}^2)$ calculation, needs retuning at each centre-of-mass energy.

7 Inclusive Particle Spectrum

The phenomenon of colour coherence in QCD implies destructive interference in soft gluon emission. This gives rise to a suppression of hadron production at small momenta. We study

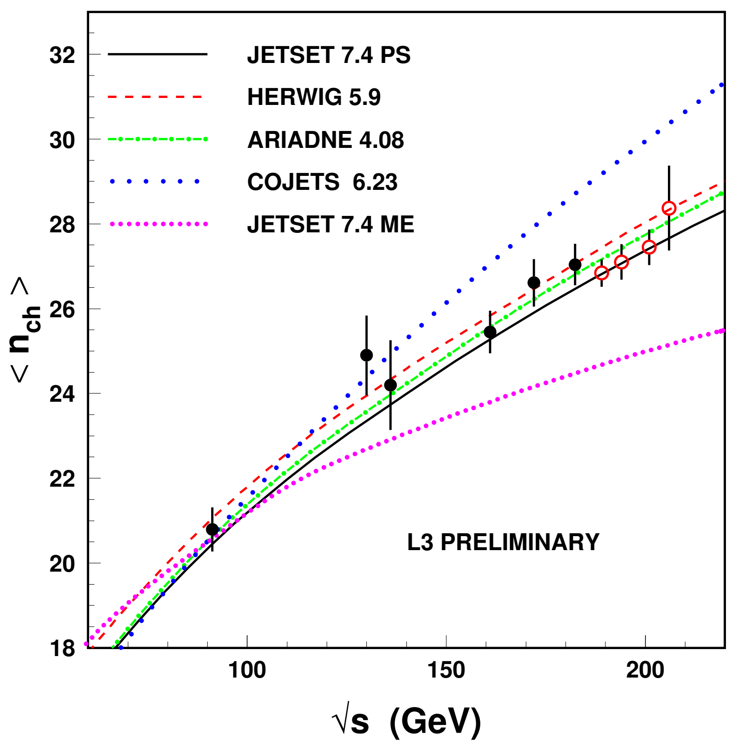

Figure 10: The mean charged particle multiplicity, $\langle \mathrm{n_{ch}} \rangle$, as a function of the centre-of-mass energy, compared to several QCD Models.

the charged particle momentum spectrum in terms of the variable $\xi = \ln(1/x)$, where x is the momentum scaled by the beam energy. The observed distribution is corrected for the effect of background, detector resolution and acceptance on a bin-by-bin basis using Monte Carlo events. The asymptotic behaviour of the ξ spectrum is predicted to be Gaussian [31,32]. With next-to-leading order corrections [33], one expects a *Platykurtic* shape (skewed Gaussian) for the ξ distribution. This implies a narrower ξ-peak shifted towards lower x-values, skewed and flattened towards higher x-values, and the tail falling off faster than Gaussian. Each of the measured ξ distributions is fitted to a Gaussian and a skewed Gaussian function restricting the fit range to values of ξ where the distribution falls to 60% of its maximum value. During the fit, the statistical errors on the measurements are taken to be uncorrelated whereas the systematic errors are taken to be maximally correlated. Both the distributions give reasonable description of the data around the peak position suggesting that the next-to-leading corrections do not influence the determination of peak position at high energies.

$<\sqrt{s}>$ (GeV)	χ^2/d.o.f.	$\xi^\star$
189.0	31.1/14	$4.06 \pm 0.01 \pm 0.03$
195.0	16.7/14	$4.13 \pm 0.02 \pm 0.03$
200.6	10.7/14	$4.16 \pm 0.02 \pm 0.04$
205.3	16.5/13	$4.16 \pm 0.03 \pm 0.06$

Table 8: Quality of fit to ξ distributions and $\xi^\star$ values at different centre-of-mass energies

The peak positions $\xi^\star$ in the ξ distribution as well as the χ^2/d.o.f. of the fits are summarised in Table 8. where the first error is statistical and the second error is due to systematics. We also include the measurements done at $\sqrt{s} = 189$ GeV. To estimate the systematic errors, we have repeated the fits changing (a) the functional form (Gaussian instead of skewed Gaussian); (b) the quality cuts on track selection; (c) the hadronic selection criteria to vary the backgrounds within one σ; (d) the model (HERWIG) used for detector corrections (the default being PYTHIA). Half of the maximum spread is assigned as the systematic error.

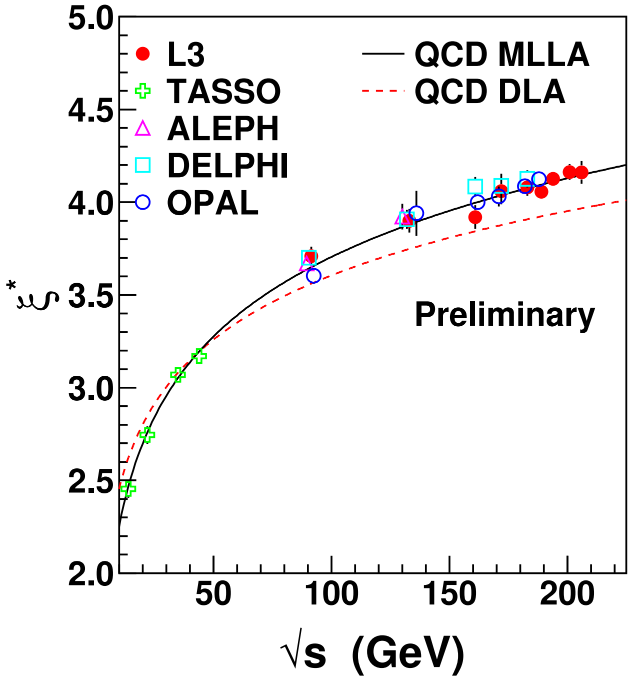

Figure 11: Energy evolution of $\xi^\star$: the solid and dashed lines are fits to the L3 and TASSO data with Modified Leading Log Approximation (MLLA) and Double Leading log Approximation (DLA) of QCD.

Figure 11 shows the measured values of $\xi^\star$ together with earlier measurements [5, 34–38] as a function of centre-of-mass energy. The energy evolution of $\xi^\star$ has been fitted using the QCD prediction:

$$\xi^\star(s) \quad = \quad Y\left(\frac{1}{2} + a\sqrt{\frac{\alpha_s(Y)}{32N_c\pi}} - a^2\frac{\alpha_s(Y)}{32N_c\pi}\right),$$

where $Y = \ln(\sqrt{s}/2\Lambda)$, $a = (11/3N_c) + (2N_f/3N_c{}^2)$, N_c and N_f are number of colours and active flavours respectively. The first term is given by the double logarithm approximation (DLA), and the correction terms arise in the next-to-leading order [39] (MLLA) QCD predictions. In the fits, we have taken the statistical error as fully uncorrelated and the systematic errors from the same experiment as fully correlated. The correlation of systematic errors among different experiments has been ignored.

We find that the data are in better agreement with QCD predictions computed to the next-to leading orders. The fit of the L3 and TASSO data to the DLA parametrisation gives a χ^2 of 56.3 for 12 degree of freedom (CL $= 1.1 \times 10^{-7}$) whereas the MLLA predictions give a fit with χ^2 of 12.2 for 12 degrees of freedom (CL $= 0.43$).

It should be recalled that the suppression of hadron production at very small momenta resulting in a bell shape of the ξ distribution is expected on purely kinematical grounds due to finite hadron masses. Soft gluon coherence, however, increases this suppression and is manifested in the energy dependence of $\xi^{\star}$. The change with energy would be approximately two times larger without any destructive interference.

8 Summary

We have measured jet rates and distributions of event shape variables in hadronic events from e^+e^- annihilation at mean centre-of-mass energies of 195.0, 200.6 and 205.3 GeV. These distributions as well as the energy dependence of the first moments of the shape variables from 30 GeV to 205.3 GeV are well described by parton shower models.

The energy dependence of the first two moments has been compared with second order perturbative QCD with power law corrections for the non-perturbative effects. The fits of the five event shape variables agree with a universal power law behaviour giving $\alpha_0 = 0.482 \pm 0.062$ (exp) $\pm$ 0.021 (th). We find a non-negligible contribution from a $\mathcal{O}(\frac{1}{s})$ term in describing the second moments of $1-T$, B_T and C.

The event shape distributions are compared to second order QCD calculations together with resummed leading and next-to-leading log terms. The data are well described by these calculations at all energies. The measurements demonstrate the running of α_{s} as expected in QCD with a value of $\alpha_{\mathrm{s}}(m_{\mathrm{Z}}) = 0.1218 \pm 0.0012$ (exp) $\pm$ 0.0061 (th). From the energy dependence of α_{s}, we determine the number of active flavours to be $N_f = 5.1 \pm 1.3$ (exp) $\pm$ 1.9 (th).

The energy evolution of the charged particle multiplicity as well as the inclusive charged particle momentum spectrum measured up to 205.3 GeV give evidence of soft gluon suppression. Energy evolution of the peak position $\xi^{\star}$ of inclusive ξ spectrum is described adequately by the next-to-leading order QCD calculation including interference effects.

References

[1] L3 Collaboration, B. Adeva *et al.*, Nucl. Inst. Meth. **A289** (1990) 35;
M. Chemarin *et al.*, Nucl. Inst. Meth. **A349** (1994) 345;
M. Acciarri *et al.*, Nucl. Inst. Meth. **A351** (1994) 300;
G. Basti *et al.*, Nucl. Inst. Meth. **A374** (1996) 293;
A. Adam *et al.*, Nucl. Inst. Meth. **A383** (1996) 342.

[2] L3 Collaboration, B. Adeva *et al.*, Phys. Lett. **B284** (1992) 471;
L3 Collaboration, O. Adriani *et al.*, Phys. Rep. **236** (1993) 1.

[3] L3 Collaboration, M. Acciarri *et al.*, Phys. Lett. **B411** (1997) 339.

[4] L3 Collaboration, M. Acciarri *et al.*, Phys. Lett. **B371** (1996) 137.

[5] L3 Collaboration, M. Acciarri *et al.*, Phys. Lett. **B404** (1997) 390;
L3 Collaboration, M. Acciarri *et al.*, Phys. Lett. **B444** (1998) 569;
L3 Collaboration, M. Acciarri *et al.*, CERN-EP/2000-064 (2000).

[6] Ariadne 4.06 Monte Carlo Program:
U. Pettersson, "ARIADNE: A Monte Carlo for QCD Cascades in the Color Dipole Formulation", Lund Preprint, LU TP 88-5 (1988);
L. Lönnblad, "The Colour Dipole Cascade Model and the Ariadne Program", Lund Preprint, LU TP 91-11 (1991).

[7] Herwig 5.9 Monte Carlo Program:
G. Marchesini and B. Webber, Nucl. Phys. **B310** (1988) 461;
I. G. Knowles, Nucl. Phys. **B310** (1988) 571;
G. Marchesini *et al.*, Comp. Phys. Comm. **67** (1992) 465.

[8] Jetset 7.4 Monte Carlo Program:
T. Sjöstrand, Comp. Phys. Comm. **82** (1994) 74.

[9] Cojets 6.23 Monte Carlo Program:
R. Odorico, Nucl. Phys. **B228** (1983) 381;
R. Odorico, Comp. Phys. Comm. **32** (1984) 139, Erratum: **34** (1985) 43;
R. Mazzanti and R. Odorico, Nucl. Phys. **B370** (1992) 23;
R. Mazzanti and R. Odorico, Bologna preprint DFUB 92/1.

[10] L3 Collaboration, B. Adeva *et al.*, Z. Phys. **C55** (1992) 39;
S. Banerjee, M. Sc. Thesis, University of Mumbai (1998).

[11] Yu. L. Dokshitzer and B. R. Webber, Phys. Lett. **B352** (1995) 451;
B. R. Webber, HEP-PH-9510283;
Yu. L. Dokshitzer *et al.*, Nucl. Phys. **B511** (1997) 396;
Yu. L. Dokshitzer *et al.*, Journal of High Energy Physics **05** (1998) 3;
Yu. L. Dokshitzer *et al.*, Eur. Phys. J. direct **C3** (1999) 1;
Yu. L. Dokshitzer, HEP-PH-9911299.

[12] Z. Kunszt and P. Nason in "Z Physics at LEP 1", CERN Report 89-08, Vol.I., p. 373.

[13] S. Catani *et al.*, Phys. Lett. **B263** (1991) 491;
S. Catani *et al.*, Phys. Lett. **B272** (1991) 368;
S. Catani *et al.*, Phys. Lett. **B295** (1992) 269;
S. Catani *et al.*, Nucl. Phys. **B407** (1993) 3;
S. Catani *et al.*, Phys. Lett. **B427** (1998) 377.

[14] Kk2f Monte Carlo Program:
S. Jadach, B. F. L. Ward and Z. Wąs, Phys. Lett. **B449** (1999) 97.

[15] The L3 detector simulation is based on GEANT Version 3.15.
See R. Brun *et al.*, "GEANT 3", CERN DD/EE/84-1 (Revised), September 1987.
The GHEISHA program (H. Fesefeldt, RWTH Aachen Report PITHA 85/02 (1985)) is used to simulate hadronic interactions.

[16] Pythia 5.7 Monte Carlo Program:
QCD parton shower and fragmentation process are taken from Jetset 7.4 [8];
T. Sjöstrand, CERN-TH-7112/93 (1993), revised august 1995;
T. Sjöstrand, Comp. Phys. Comm. **82** (1994) 74.

[17] R. Engel, Z. Phys. **C66** (1995) 203;
R. Engel, J. Ranft and S. Roesler, Phys. Rev. **D52** (1995) 1459.

[18] S. Jadach, B. F. L. Ward and Z. Wąs, Comp. Phys. Comm. **79** (1994) 503.

[19] J. H. Field, Phys. Lett. **B323** (1994) 432;
J. H. Field and T. Riemann, Comp.Phys.Comm. **94** (1996) 53.

[20] S. Jadach *et al.*, Phys. Lett. **B390** (1997) 298.

[21] M. Skrzypek *et al.*, Comp. Phys. Comm. **94** (1996) 216;
M. Skrzypek *et al.*, Phys. Lett. **B372** (1996) 289.

[22] Yu. L. Dokshitzer, Contribution to the Workshop on Jets at LEP and HERA (1990);
N. Brown and W. J. Stirling, Rutherford Preprint RAL-91-049;
S. Catani *et al.*, Phys. Lett. **B269** (1991) 432;
S. Bethke *et al.*, Nucl. Phys. **B370** (1992) 310.

[23] JADE Collaboration, W. Bartel *et al.*, Z. Phys. **C33** (1986) 23;
JADE Collaboration, S. Bethke *et al.*, Phys. Lett. **B213** (1988) 235.

[24] Yu. L. Dokshitzer *et al.*, hep-ph/9707323 (1997).

[25] S. Catani and M. Seymour, Phys. Lett. **B378** (1996) 287.

[26] Yu. L. Dokshitzer and B. R. Webber, Phys. Lett. **B404** (1997) 321;
B. R. Webber, Nucl. Phys. Proc. Suppl. **71** (1999) 66;
G. Salam, private communication.

[27] Particle Data Group, C. Caso *et al.*, Eur. Phys. J. **C3** (1998) 1.

[28] ALEPH Collaboration, D. Decamp *et al.*, Phys. Lett. **B273** (1991) 181;
ALEPH Collaboration, D. Buskulic *et al.*, Z. Physik **C55** (1992) 209;
DELPHI Collaboration, P. Aarnio *et al.*, Phys. Lett. **B240** (1990) 271;
DELPHI Collaboration, P. Abreu *et al.*, Z. Phys. **C50** (1991) 185;
OPAL Collaboration, M. Z. Akrawy *et al.*, Z. Phys. **C47** (1990) 505;
OPAL Collaboration, P. D. Acton *et al.*, Z. Phys. **C53** (1992) 539.

[29] ALEPH Collaboration, D. Buskulic *et al.*, Z. Physik **C73** (1997) 409;
ALEPH Collaboration, R. Barate *et al.*, Phys. Rep. **294** (1998) 1;
DELPHI Collaboration, P. Abreu *et al.*, Phys. Lett. **B372** (1996) 172;
DELPHI Collaboration, P. Abreu *et al.*, Z. Physik **C73** (1997) 229;
DELPHI Collaboration, P. Abreu *et al.*, Phys. Lett. **B416** (1998) 233;
OPAL Collaboration, G. Alexander *et al.*, Z. Physik **C72** (1996) 191;
OPAL Collaboration, K. Ackerstaff *et al.*, Z. Physik **C75** (1997) 193.

[30] AMY Collaboration, Y. K. Li *et al.*, Phys. Rev. **D41** (1990) 2675;
AMY Collaboration, H. W. Zheng *et al.*, Phys. Rev. **D42** (1990) 737;
JADE Collaboration, W. Bartel *et al.*, Z. Phys. **C20** (1983) 187;
MARK J Collaboration, D. P. Barber *et al.*, Phys. Rev. Lett. **43** (1979) 901;
TASSO Collaboration, W. Braunschweig *et al.*, Z. Phys. **C45** (1989) 193;
TASSO Collaboration, W. Braunschweig *et al.*, Z. Phys. **C47** (1990) 187;

M. Yamauchi (TOPAZ Collaboration), ‘Recent Results from TOPAZ at TRISTAN’, 24th Int. Conf. on High Energy Physics, Munich 1988.

[31] A. H. Mueller, in *Proc. 1981 International Symposium on Lepton and Photon Interactions at High Energies*, ed. W. Pfeil (Bonn, 1981), p.689; Yu. L. Dokshitzer, V. S. Fadin and V. A. Khoze, Phys. Lett. **B115** (1982) 242.

[32] A. H. Mueller, Nucl. Phys. **B213** (1983) 85, *ibid.* **B241** (1984) 141.

[33] C. P. Fong and B. R. Webber, Phys. Lett. **B229** (1989) 289.

[34] L3 Collaboration, B. Adeva *et al.*, Phys. Lett. **B259** (1991) 199.

[35] TASSO Collaboration, W. Braunschweig *et al.*, Z. Physik **C47** (1990) 187.

[36] ALEPH Collaboration, R. Barate *et al.*, Phys. Rep. **294** (1998) 1.

[37] DELPHI Collaboration, P. Abreu *et al.*, Phys. Lett. **B275** (1992) 231;
DELPHI Collaboration, P. Abreu *et al.*, Z. Physik **C73** (1997) 229;
DELPHI Collaboration, P. Abreu *et al.*, Phys. Lett. **B459** (1999) 397.

[38] OPAL Collaboration, M. Akrawy *et al.*, Phys. Lett. **B247** (1990) 617;
OPAL Collaboration, G. Alexander *et al.*, Z. Physik **C72** (1996) 191;
OPAL Collaboration, K. Ackerstaff *et al.*, Z. Physik **C75** (1997) 193;
OPAL Collaboration, G. Abbiendi *et al.*, CERN-EP/99-178 (1999).

[39] Yu. L. Dokshitzer *et al.*, Basics of Perturbative QCD, Editions Frontieres, Gif-sur-Yvette, 1991.